

Supplementary Information

Geometry-dependent compressive responses in nanoimprinted submicron-structured shape memory polyurethane

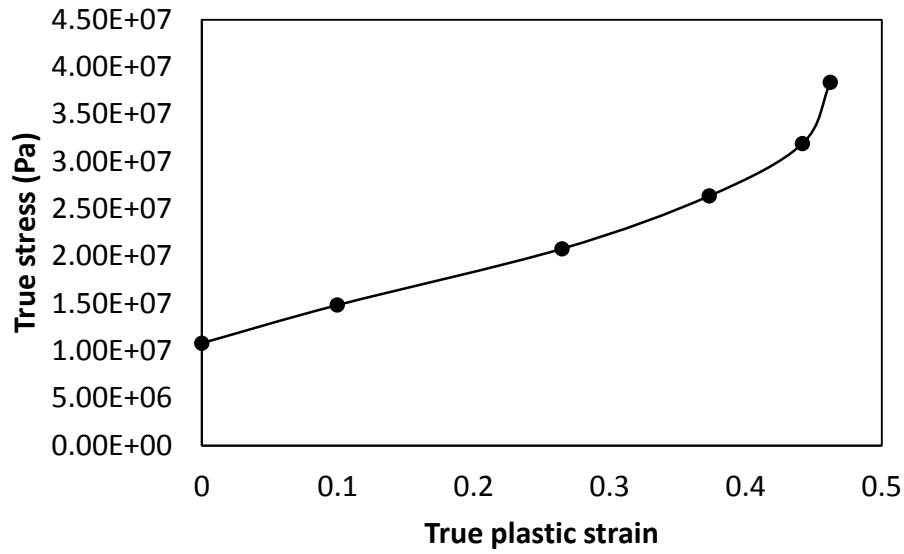
Wei Li Lee^{a,b}, Hong Yee Low^{b,*} and Christine Ortiz^{a,*}

^aDepartment of Materials Science and Engineering, Massachusetts Institute of Technology, 77
Massachusetts Avenue, Cambridge, MA 02139, United States

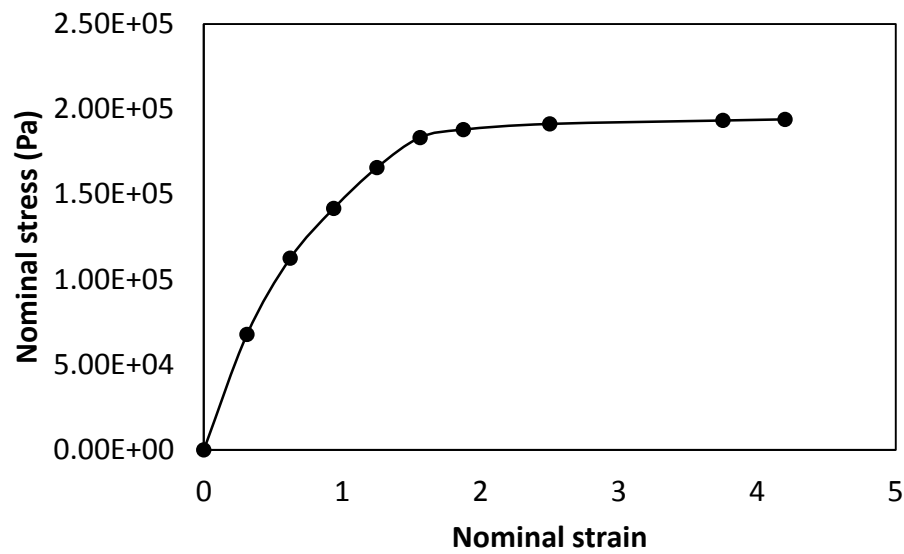
^bEngineering Product Development, Singapore University of Technology and Design, 8
Somapah Road, Singapore 487372, Singapore

*hongyee_low@sutd.edu.sg

*cortiz@mit.edu



(a)



(b)

Figure S1. (a) Yield stress-yield strain curve at room temperature. (b) Uniaxial nominal stress-strain curve at 90 °C.

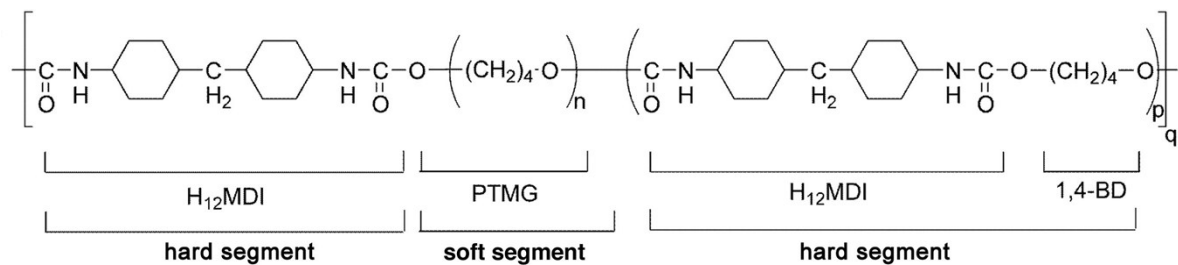
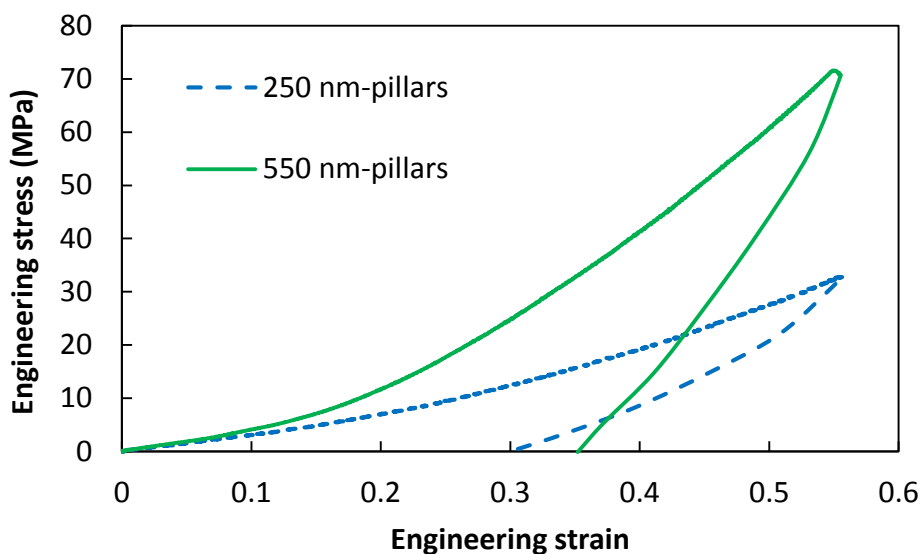
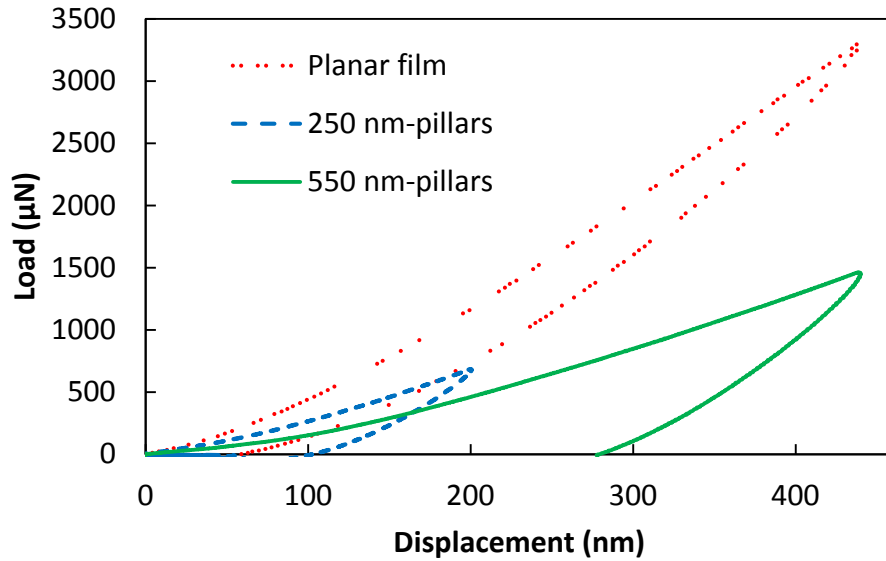


Figure S2. Chemical structure of the shape memory thermoplastic elastomer Tecoflex EG72D. It is synthesized from methylene bis(*p*-cyclohexyl isocyanate) (H₁₂MDI), 1,4-butanediol (BD), and poly(tetramethylene glycol) (PTMG).



(a)



(b)

Figure S3. (a) Stress-strain curves in a loading-unloading cycle in compression of 250 nm-pillars and 550 nm-pillars by a flat punch diamond indenter. (b) Load-displacement curves of displacement-controlled indentation. The strain rate and maximum compressive strain attained before unloading are 0.1 s^{-1} and 55%, respectively,

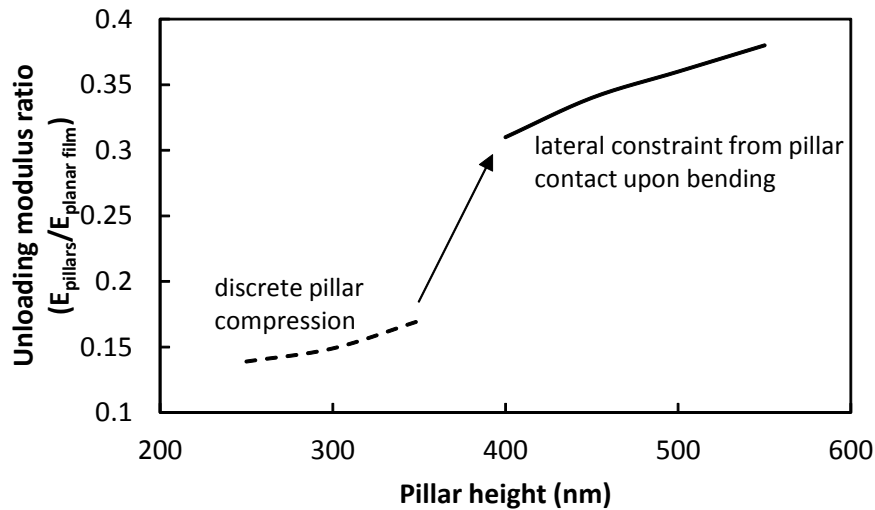


Figure. S4. FEA predictions of unloading modulus ratio as a function of pillar height.

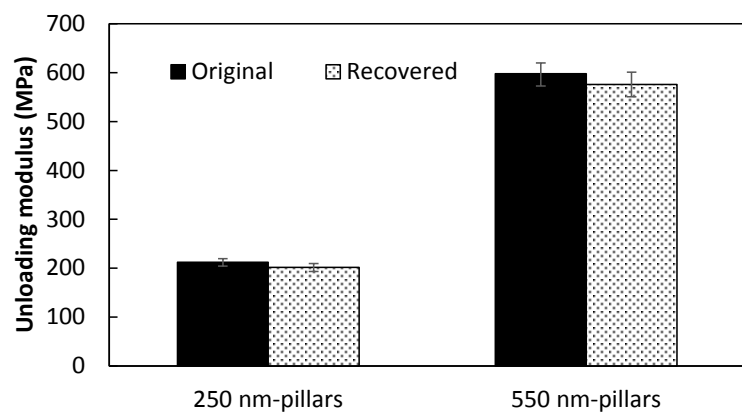


Figure S5. Unloading modulus values of the original and recovered patterns after five cycles of load-unloading.

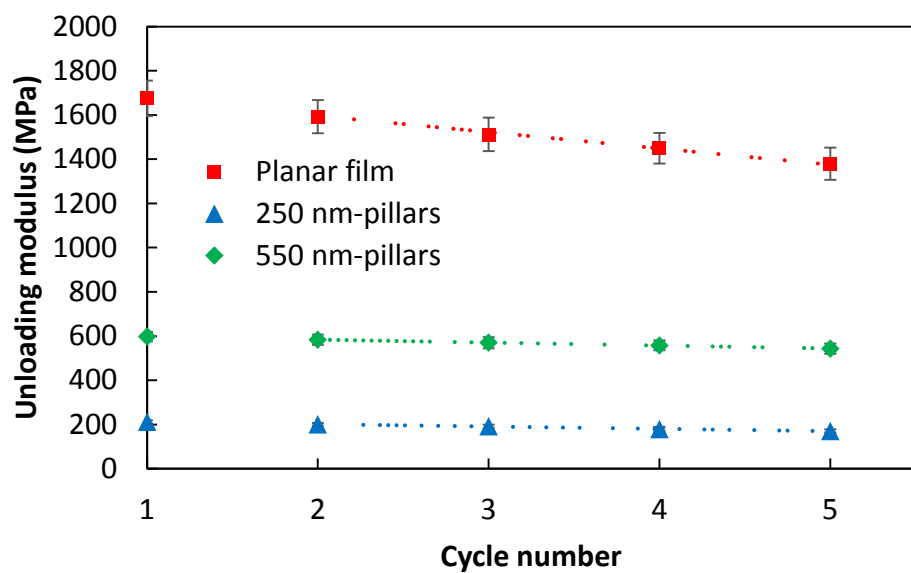


Figure S6. Changes in the unloading modulus as a function of loading-unloading cycles.

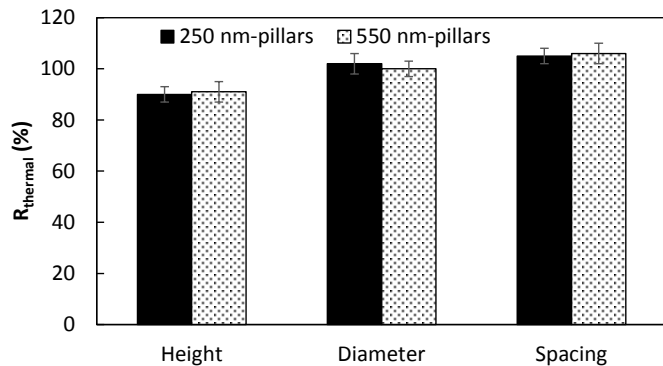
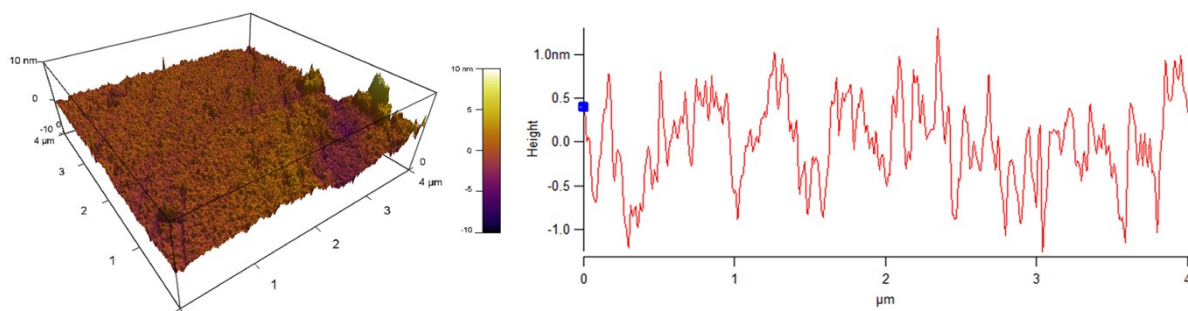
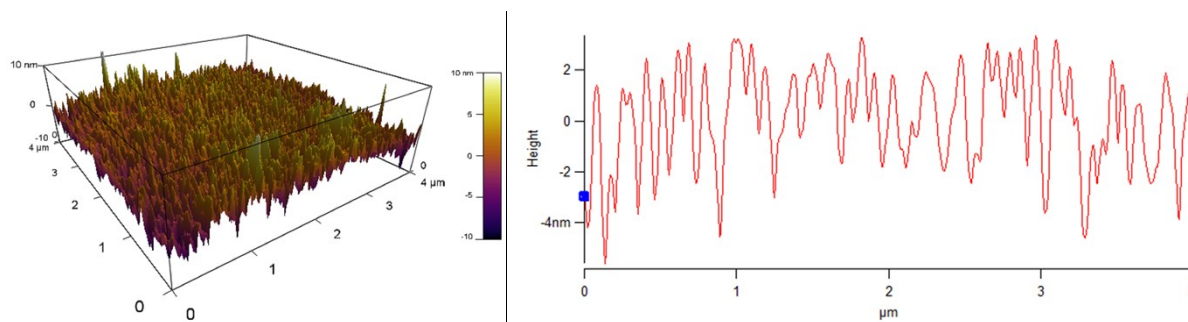


Figure S7. The calculated recovery percentage ($R_{\text{thermal}} = \text{Recovered dimension} / \text{Original dimension} \times 100\%$) after one cycle of shape programming at 200% strain and thermal recovery for the 250 nm- and 550 nm-pillars.

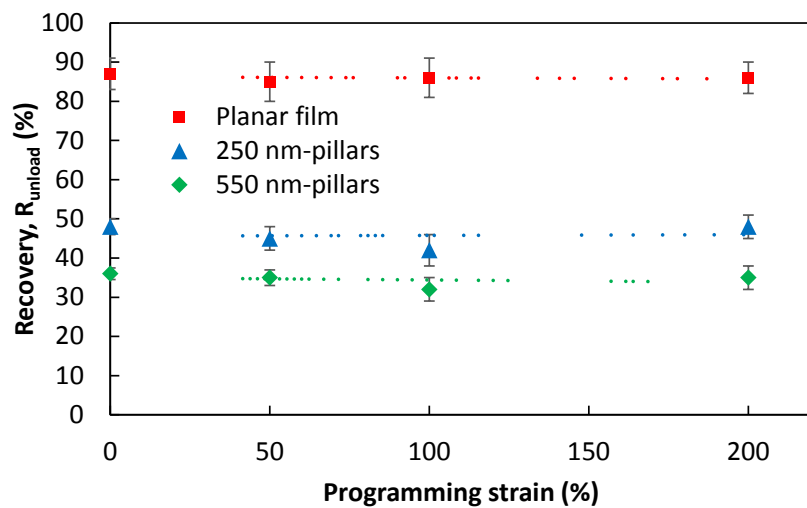


(a)

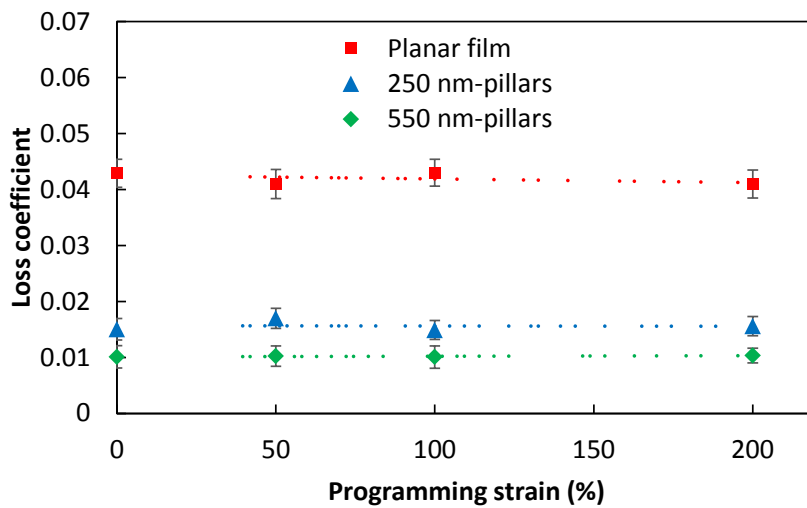


(b)

Figure S8. Topographic AFM images and the corresponding height profiles of (a) original (unstretched) planar film and (b) 200% stretched planar film.



(a)



(b)

Figure S9. Changes in the (a) elastic recovery (b) loss coefficient as a function of programming tensile strain for the planar film, 250 nm-pillars and 550 nm-pillars.

Table S1. Dimensional analyses (mean \pm standard deviation for $n > 60$ measurements) of 250 nm- and 550 nm-pillars under different tensile strains.

Pillar system	Macroscopic applied tensile strain (%)	Width of the top surface along stretching (nm)	Width of the top surface orthogonal to stretching (nm)	Width of the bottom surface along stretching (nm)	Width of the bottom surface orthogonal to stretching (nm)	Height (nm)	Pillar areal density (μm^{-2})
250 nm-pillars	0 (as-imprinted)	227 \pm 5	228 \pm 6	235 \pm 4	229 \pm 5	248 \pm 5	8.68
	50	232 \pm 4	225 \pm 5	351 \pm 6	222 \pm 6	238 \pm 4	7.03
	100	240 \pm 5	220 \pm 5	395 \pm 7	216 \pm 6	225 \pm 5	5.54
	200	258 \pm 7	213 \pm 6	550 \pm 9	209 \pm 8	196 \pm 15	4.50
550 nm-pillars	0 (as-imprinted)	232 \pm 7	234 \pm 10	238 \pm 8	231 \pm 7	553 \pm 10	8.26
	50	238 \pm 8	235 \pm 7	379 \pm 10	225 \pm 7	517 \pm 15	7.07
	100	240 \pm 5	229 \pm 5	403 \pm 9	219 \pm 6	495 \pm 14	5.83
	200	253 \pm 9	224 \pm 6	562 \pm 10	212 \pm 7	430 \pm 18	4.82